Elementary reactions and a mechanism for the suppression of hydrogen fires by CF_3I

Paul Marshall,[a,b] Ashutosh Misra,[a] Jessie Yuan,[a] Rajiv Berry[b] and Andrew McIlroy[c]

[a]University of North Texas, Department of Chemistry, P.O. Box 5068, Denton TX 76203

[b]Center for Computational Modeling of Nonstructural Materials, Wright Laboratory, Wright-Patterson AFB, OH 45433

[c]SandiaNational Laboratories, Combustion Research Facility, P.O. Box 969, MS 9051, Livermore, CA 94551-0969

Abstract

Concentration profiles of stable species in low-pressure hydrogen-oxygen flames were characterized by microprobe sampling with mass spectrometric detection. This system was employed to investigate the effects of doping with CF_3I. Essentially no inhibition was observed. The observations were rationalized in terms of a 67-step mechanism, which included 24 iodine reactions. Rate constants for these iodine reactions were determined by the flash photolysis/time-resolved resonance fluorescence method, and by high level ab initio quantum calculations which characterized the potential energy surfaces, together with literature data and empirical estimates. The ab initio results agreed well with other elementary rate constant information. The flame modeling gave good accord with experiment, and revealed that in the preheat zone [H] is lowered by a cycle involving CF_3I, H and HI, but that in the combustion zone [H] is largely unaffected.

Introduction

CF_3I is a promising fire suppression agent for some applications, and a potential substitute for CF_3Br, because CF_3I is degraded rapidly in the atmosphere and therefore possesses negligible ozone depletion and global warming potentials. A barrier to our understanding and prediction of its performance has been a lack of reliable kinetic and thermochemical parameters for the quantitative modeling of iodine combustion inhibition. Here the chemistry of CF_3I in hydrogen-oxygen flames is considered in detail. Hydrogen flames are of scientific interest because they are simple, well-characterized, and the hydrogen reaction mechanism is an important subset of any hydrocarbon mechanism. Hydrogen fire suppression is of practical importance for hydrogen-fueled space launch vehicles, hydrogen-rich streams in petroleum refining, and for the development of a practical hydrogen-based economy.

The work presented was conducted in several phases. First, new measurements of the elementary reactions of CF_3I with the flame species H, OH and O have been made. Second, high-level quantum chemical calculations have been carried out for these and other iodine reactions. These calculations characterized the thermochemistry and reactivity of transient intermediates such as IO and HOI, as well as key inhibition reactions of I and HI. Third, the results were combined to construct an overall $H_2/O_2/CF_3I$ combustion mechanism which was tested by comparison of modeling results with new low pressure flame measurements of CF_3I-seeded $H_2/O_2/Ar$ flames.

The results show that CF_3I is a poor inhibitor of H_2/O_2 flames, and provide a test of a subset of reactions needed for modeling the suppression of hydrocarbon flames by iodine species

Individual Reaction Measurements

The elementary reactions

$$CF_3I + H \rightarrow CF_3 + HI \quad (1)$$

$$CF_3I + OH = CF_3 + HOI \quad (2)$$

$$CF_3I + O = CF, + IO \quad (3)$$

were studied by the pulsed photolysis - resonance fluorescence technique. Radicals were generated by flash lamp and/or excimer laser photolysis of precursors (NH_3 for H atoms, H_2O for OH and **O,** and ***SO,*** for **O)** on a microsecond or shorter time scale, in the presence of a large excess of CF_3I. The radicals then reacted under pseudo-first-order conditions over millisecond time scales. For example, for reaction 1:

$$d[H]/dt = -k_1[H][CF_3I] - k_{diff}[H] = -k_{ps1}[H]$$

where k, and b a r e the rate constants for reaction with CF_3I and loss by diffusion, respectively. Linear plots of the pseudo-first-order rate constant k_{ps1} versus $[CF_3I]$ yielded **k,** as the slope. Because the radical concentration was kept very small, below about 10^{12} molecule cm^{-3}, self-reaction and consumption by photolysis or reaction products was minimized, ***so*** that the desired elementary reactions were *isolated* from competing processes. The radical concentration was monitored **as** a function of time with microsecond resolution by means of UV or vacuum UV resonance fluorescence excited by a microwave-powered lamp. The fluorescence signals were detected via photon counting and averaged over typically 100-500 radical decays. **A** diagram of the apparatus at the University of North Texas is shown below in Fig. 1.

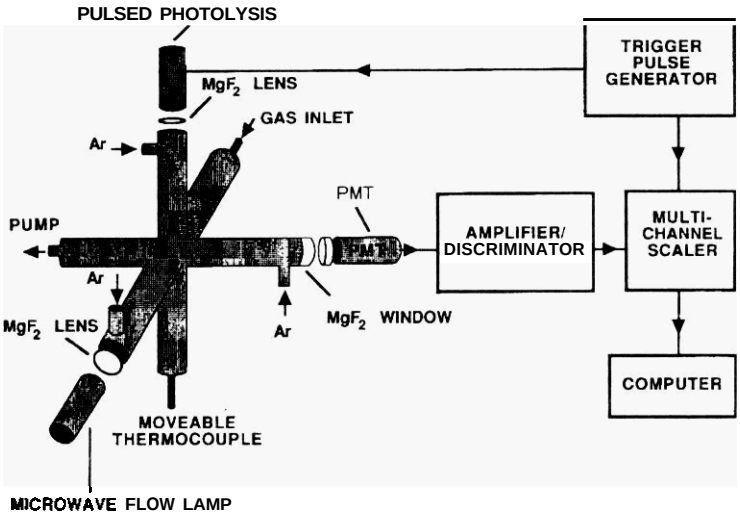

Fig. 1. Schematic diagram **of** the flash-photolysis resonance fluorescence apparatus.

Figure 2 illustrates the rate constants obtained for reactions **1-3** in Arrhenius form The present work represents the first measurements above room temperature for reactions 1 and 2, and extends the data available for reaction **3** to considerably higher temperatures. Our

measurements are Summarized here (all mors ±1σ and represent statistical uncertainties only):

$k_1 = (6.8 \pm 0.2) \times 10^{-11} \exp(-4.0 \pm 0.1 \text{ kJ mol}^{-1}/RT)$ cm^3 molecule^{-1} s^{-1} (295-730 K)

$k_2 = (1.0 \pm 0.2) \times 10^{-11} \exp(-12.7 \pm 0.6 \text{ kJ mol}^{-1}/RT)$ cm^3 molecule^{-1} s^{-1} (280-440 K)

$k_3 = (1.7 \pm 0.1) \times 10^{-11} \exp(-2.6 \pm 0.1 \text{ kJ mol}^{-1}/RT)$ cm^3 molecule^{-1} s^{-1} (295-715 K)

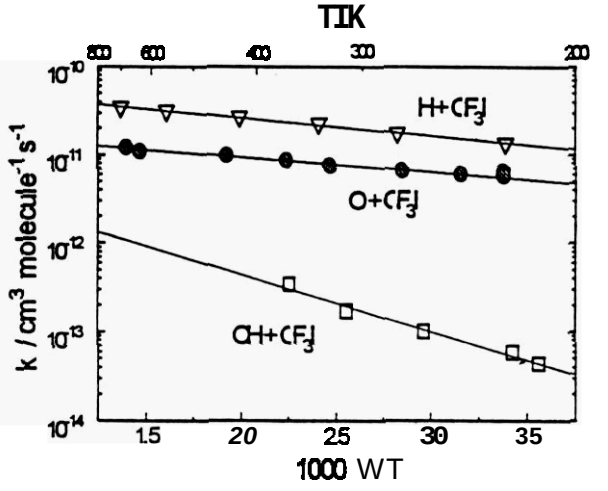

Fig. 2 Arrhenius plot of CF_3I isolated reaction measurements.

Ab Initio Calculations

Gaussian-2 (G2) theory, as extended to iodine-containing species,[1] was applied at the Wright Laboratory to characterize reactants, products and transition states (TSs) for individual reactions likely to be important in CF_3I inhibition of hydrogen combustion Briefly, molecular geometries and vibrational frequencies were obtained at the MP2/6-31G(d) level of theory[2] and were employed to compute the partition functions Q for each species. The TS geometries are shown in Fig. 3.

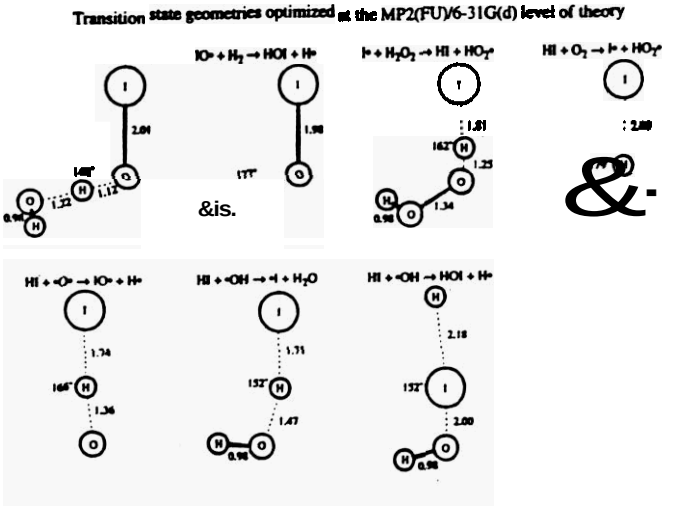

Fig. 3. Computed transition state geometries.

Single-point energies were computed at the G2 level of theory, which approximates a complete QCISD(T)/6-311+G(3d,2p) calculation, and used to derive reaction enthalpies and energy barriers E_0[3]. The ab initio data were employed in canonical transition state theory?

$$k_{TST} = \Gamma \frac{k_B T}{h} \frac{Q_{TS}}{Q_{reactants}} \exp(-\frac{E_0^{\ddagger}}{RT})$$

Γ is a correction term for quantum mechanical tunneling, and hindered internal rotors are also treated in this analysis. Rate constants for the following processes were obtained:

$O + HI \rightarrow OH + I$
$HI + O_2 \rightarrow I + HO_2$
$I + H_2O_2 \rightarrow HI + HO_2$
$IO + H_2 \rightarrow HOI + H$
$H_2O + IO \rightarrow OH + HOI$

The computational results are plotted in Arrhenius form on Fig. 4. The rate constant for O + HI → OH + I is already known experimentally, and as may be seen from Fig. 4 there is excellent accord between theory and experiment for this reaction. No reaction barrier was found for OH + HI → H_2O + I, in accord with recent measurements, nor for the reaction HOI + H → OH + HI which accordingly was assumed to be fast.

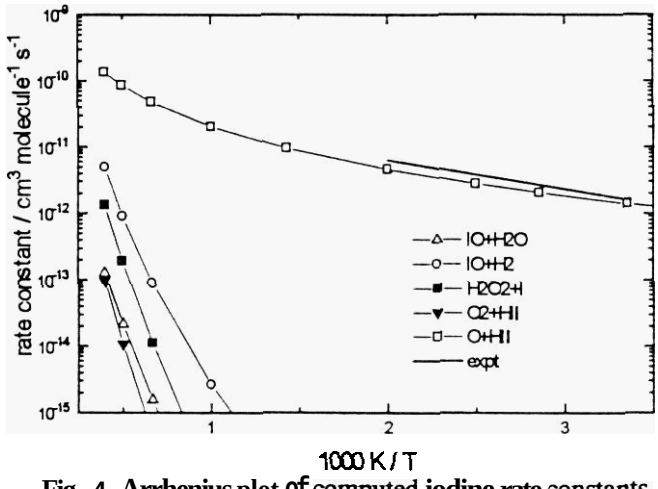

Fig, 4. Arrhenius plot of computed iodine rate constants.

Reactions 1-3 were also analyzed. The computed energy barrier for reaction 1 was within 5 kJ mol^{-1} of that measured. Reaction 2 was found to proceed with no barrier beyond the endothermicity. This means that the measured activation energy, together with the known thermochemistry of CF_3I, OH and CF_3, yields an estimate for $\Delta_f H_{298}$(HOI), of -70 ± 7 kJ mol-'. This value compares well with our computed value of -65 kJ mol-'. Reaction 3 was found to proceed via a bound CF_3IO intermediate, which under combustion conditions will dissociate to CF_3 + IO.

Flame Measurements

A 30 torr stoichiometric $H_2/O_2/Ar$ flame was employed, with molar ratios of 0.54/0.27/1.61. This flame was analyzed to investigate the effects of doping with 0.6% CF_3I by

mole. The stable species H_2, O_2, Ar, CF_3I and HF were detected via a microprobe sampling mass spectrometer. A diagram of the apparatus at the Aerospace Corporation is shown in Fig. **5.**

Experimental Layout

+Corrosion resistant construction

♦Mulitiple diagnostics
- +Mass spectrometer
- +Laser induced fluorescence
- +Thermocouple

♦Servo control of flow rates and pressure

+Three axis burner positioning

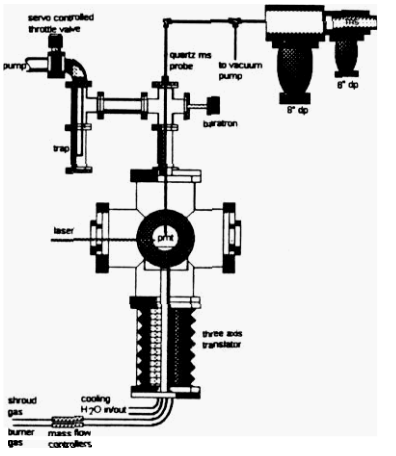

Fig. 5. The flame sampling apparatus.

Figure 6 shows examples of measured profiles of concentration versus height above the burner.

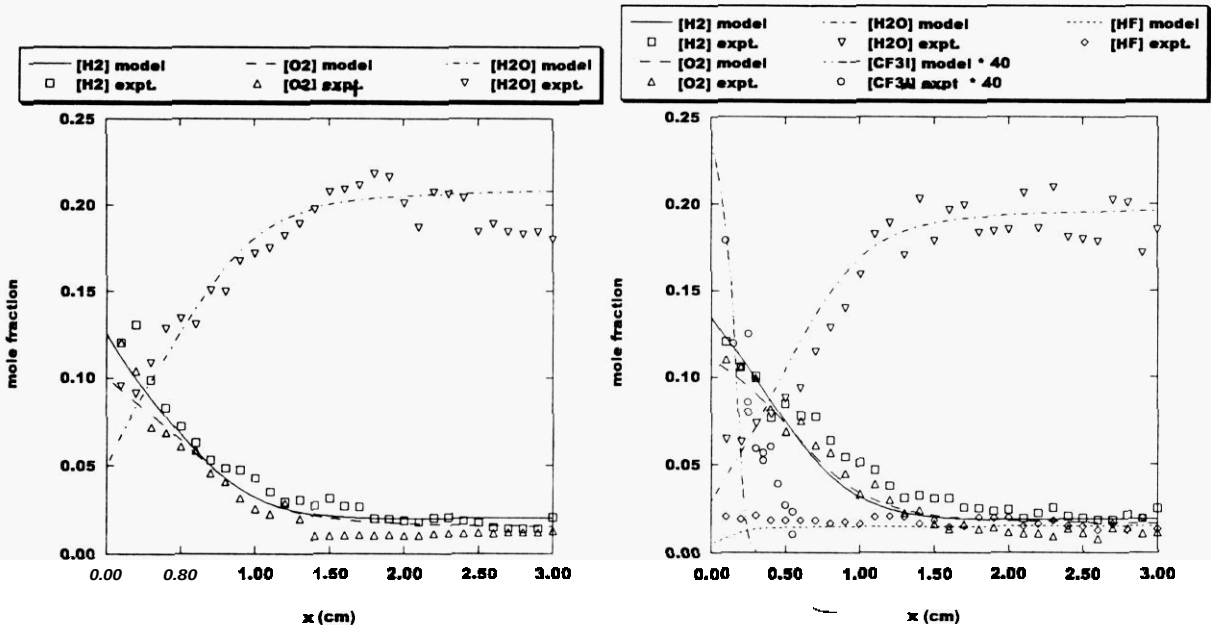

Fig. 6. Measured and computed concentration **profiles in undoped (left) and** doped **(right) flames.**

The profiles for stable species in the doped and undoped flames looked quite similar. Within the experimental uncertainty, CF_3I had no effect on the hydrogen flame. The CF_3I is clearly destroyed early in the flame preheat zone and HF appears at fairly constant concentration throughout the flame, probably largely due to diffusion.

Flame Modeling

The flame concentration profiles were compared to values calculated with the Sandia PREMIX laminar flame code, using a mechanism constructed from the measurements and computations discussed above, literature data, and guesses for some processes based on chlorine or bromine analogs where no other data were available. This mechanism is summarized below.

	REACTIONS CONSIDERED			A	b	E
1.	H2+O2=2OH			1.70E+13	.0	47180.0
2.	H2+OH=H2O+H			1.17E+09	1.3	3626.0
3.	H+O2=OH+O			5.13E+16	-.8	16507.0
4.	O+H2=OH+H			1.80E+10	1.0	8826.0
5.	H+O2+M=HO2+M			2.10E+18	-1.0	.0
	H2O	Enhanced by	2.100E+01			
6.	H+O2+O2=HO2+O2			6.70E+19	-1.4	.0
7.	OH+HO2=H2O+O2			5.00E+13	.0	1000.0
8.	H+HO2=2OH			2.50E+14	.0	1900.0
9.	O+HO2=O2+OH			4.80E+13	.0	1000.0
10.	2OH=O+H2O			6.00E+08	1.3	.0
11.	H+H+M=H2+M			1.00E+18	-1.0	.0
12.	H+H+H2=2H2			9.20E+16	-.6	.0
13.	H+H+H2O=H2+H2O			6.00E+19	-1.3	.0
14.	2O+M=O2+M			1.41E+17	-1.0	398.0
15.	H+OH+M=H2O+M			7.50E+23	-2.6	.0
	H2O	Enhanced by	2.000E+01			
16.	H+HO2=H2+O2			2.50E+13	.0	700.0
17.	HO2+HO2=H2O2+O2			2.00E+12	.0	.0
18.	H2O2+M=2OH+M			1.30E+17	.0	45500.0
19.	H2O2+H=HO2+H2			1.60E+12	.0	3800.0
20.	H2O2+OH=H2O+HO2			1.00E+13	.0	1800.0
21.	H+HF=H2+F			2.19E+14	.0	33740.0
22.	H+F2=HF+F			1.20E+14	.0	2400.0
23.	F+F+M=F2+M			1.00E+14	.0	.0
24.	H+F+M=HF+M			9.55E+17	-1.0	.0
25.	CF3+H=HF+CF2			3.98E+12	.0	.0
26.	CF3+O=CF2:O+F			1.29E+14	.0	2000.0
27.	CF3+OH=CF2:O+HF			3.98E+12	.0	.0
28.	CF3+O2=CF3O+O			2.26E+09	1.1	21500.0
29.	CF3O+M=CF2:O+F			9.03E+26	-3.4	21100.0
30.	CF3O+H=CF2:O+HF			1.00E+14	.0	.0
31.	CF3O+H2=>CF3OH+H			1.00E+13	.0	5000.0
32.	CF3O+H2O=>CF3OH+OH			0.00E+00	.0	5000.0
33.	CF3OH=>CF2:O+HF			1.00E+14	.0	43000.0
34.	CF2:O+H=CF:O+HF			1.29E+11	.0	.0
35.	CF2+H=HF+CF			1.00E+13	.0	.0
36.	CF2+O=CF:O+F			1.00E+13	.0	.0
37.	CF2+OH=CF:O+HF			1.00E+13	.0	.0
38.	CF2+OH=CF2:O+H			1.00E+13	.0	.0
39.	CF:O+M=F+CO+M			1.44E+14	.0	30000.0
40.	CF:O+H=HF+CO			2.00E+14	.0	.0
41.	CF:O+O=CO+FO			1.00E+14	.0	.0
42.	CF:O+OH=CO+HFO			1.00E+14	.0	.0
43.	CF:O+OH=CO2+HF			1.00E+14	.0	.0
44.	CF3I+M=CF3+I+M			1.95E+15	.0	34350.0
45.	CF3I+H=CF3+HI			4.09E+13	.0	950.0
46.	CF3I+O=CF3+IO			1.02E+13	.0	620.0
47.	CF3I+OH=CF3+HOI			1.75E+08	1.5	1910.0
48.	CF3I+I=CF3+I2			7.40E+13	.0	11800.0
49.	I2+M=I+I+M			8.25E+13	.0	30300.0
50.	H+I2=HI+I			4.31E+14	.0	430.0
51.	O+I2=IO+I			8.43E+13	.0	.0
52.	OH+I2=HOI+I			1.08E+14	.0	.0

53. H+HI=H2+I	4.74E+13	.0	660.0
54. O+HI=OH+I	1.51E+07	2.0	.0
55. OH+HI=H2O+I	3.61E+13	.0	.0
56. H+I+M=HI+M	1.92E+21	-1.9	.0
57. I+HO2=HI+O2	9.03E+12	.0	2170.0
58. I+H2O2=HI+HO2	2.29E-03	4.7	17630.0
59. IO+O=I+O2	1.81E+13	.0	.0
60. IO+H=OH+I	1.81E+13	.0	.0
61. IO+OH=HO2+I	1.81E+13	.0	.0
62. IO+H2=HOI+H	2.09E-09	6.4	5650.0
63. IO+HO2=HOI+O2	3.85E+13	.0	.0
64. HOI+O=IO+OH	1.50E+13	.0	.0
65. HOI+OH=IO+H2O	6.00E+12	.0	.0
66. IO+H2O2=HOI+HO2	6.00E+12	.0	.0
67. HOI+M=OH+I+M	6.00E+13	.0	50000.0

NOTE: A units mole-cm-sec-K, E units cal/mole

Figure *6* shows comparisons of computed and measured concentration profiles, which are in reasonable accord. Computed profiles for other halogenated species are given in Fig. 7.

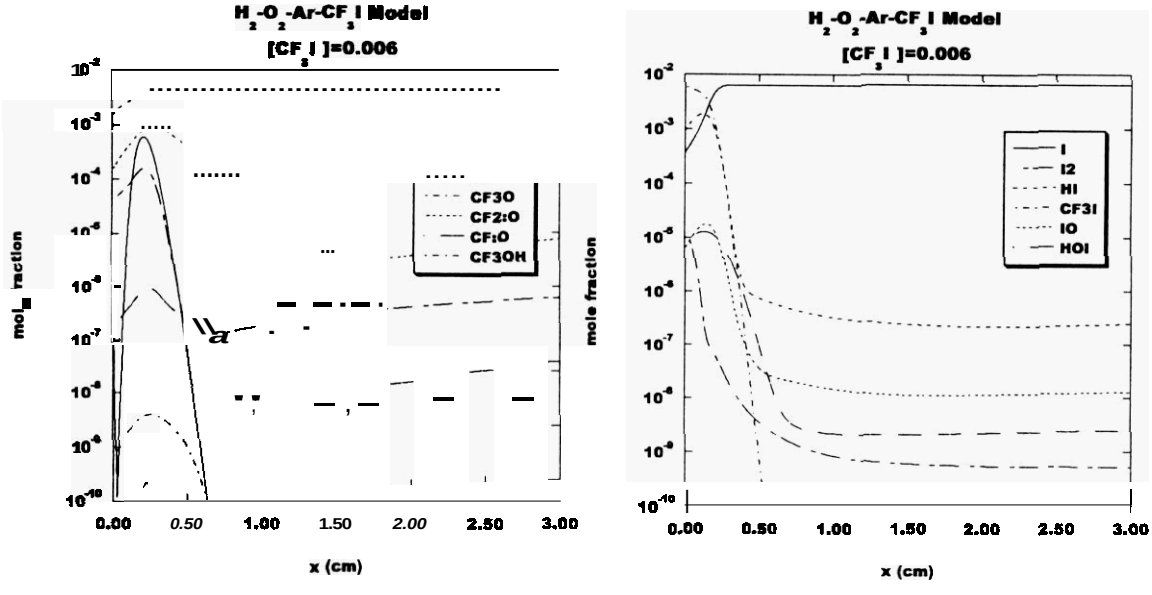

Fig. 7. Modeled flame profiles of **halogenated species in a $CF_3I/H_2/O_2$ flame**

Figure 8 overleaf shows the reactive **flux** through the various iodine reactions in the mechanism. In the preheat zone (the first 0.5 cm above the burner, where the temperature is below 800 K) the three dominant reactions form a radical-consuming *cycle:*

$$CF_3 + I + M \rightarrow CF_3I + M$$
$$H + CF_3I \rightarrow CF_3 + HI$$
$$H + HI \rightarrow H_2 + I$$
$$H + H \rightarrow H_2$$

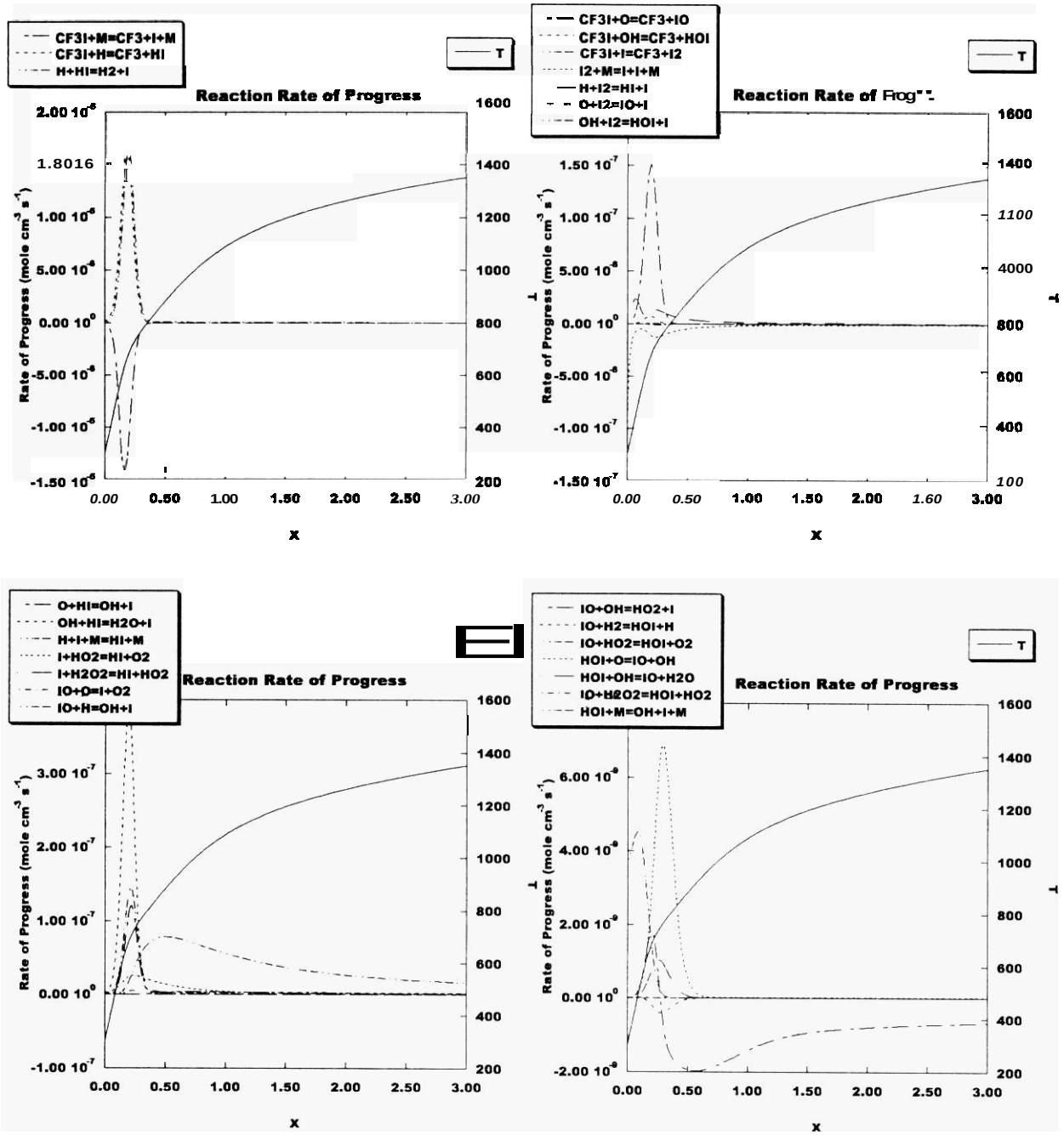

Fig, 8. Computed reaction fluxes (left axis) and temperature **profile** (right **axis)** as a function of height above the **burner for** iodine reactions in a CF_3I-doped H_2/O_2 flame.

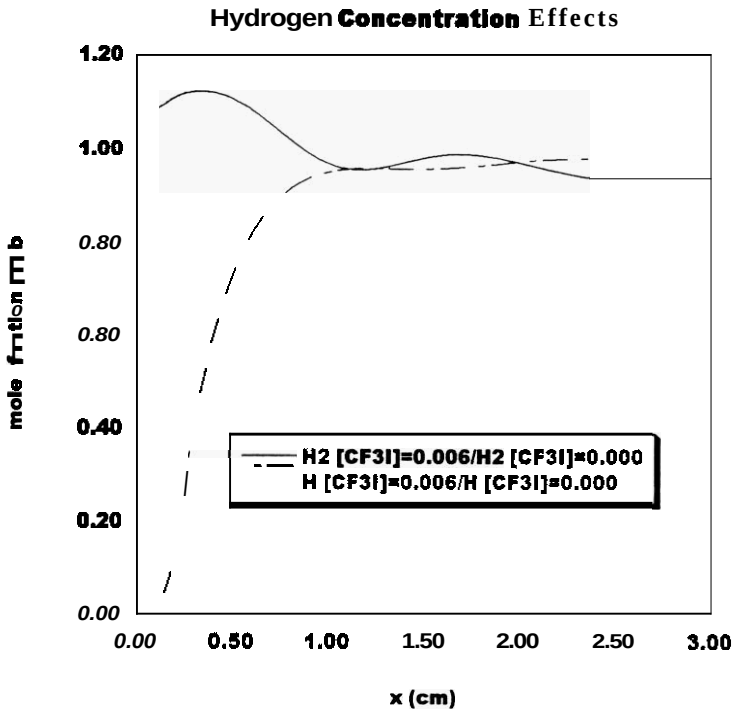

Fig. 9. Reduction of [H] by the CF_3I-initiated cycle in the preheat region.

As shown in Fig. 9, the impact of this cycle is to lower the concentration of H atoms dramatically, with respect to values in the preheat zone of an undoped flame. Higher temperatures in the combustion zone make CF_3I and HI formation unfavorable and this cycle no longer operates there. The dominant form of iodine becomes the atomic state. Other iodine species such as IO and HOI are apparently not stable enough to be involved in significant cycles that might deplete the radical pool and suppress the flame. This can be contrasted to hydrocarbon flames, where addition of half the fraction of CF_3I used here caused significant combustion inhibition.'

Conclusions

Measurements of isolated elementary reactions and ab initio quantum calculations have been employed to construct a mechanism for the chemistry of CF_3I. This mechanism has been used to predict the behavior of CF_3I in a hydrogen-oxygen flame. There is good accord with concentration profiles of stable species measured by mass spectrometry in a low-pressure hydrogen-oxygen flame. The analysis reveals that early in the flame [H] is lowered by a cycle involving CF_3I, H and HI, but that in the combustion zone [H] is largely unaffected. The consequence is that CF_3I, like CF_3Br, is overall a poor inhibitor of hydrogen combustion.

Acknowledgments

The flame measurements at Aerospace Corp. were conducted with the assistance of Brian Brady. This work was supported in part by the Aerospace Sponsored Research Program, the R. A. Welch Foundation, the U.S. Department of Energy (Basic Energy Sciences) and the U.S. **Air** Force.

References

1. M. N. Glukhovtsev, A. Pross, M. P. McGrath and L. Radom, L. *J. Chem.* ***Phys.*****, 103, 1878 (1995).**
2. M. J. Frisch, G. W. Trucks, H. B. Schlegel, P. M. W. Gill, B. G. Johnson, M. A. Robb, J. R. Cheeseman, T. Keith, G. A. Petersson, J. A. Montgomery, K. Raghavachari, M. A. Al-Laham, V. G. Zakrzewski, J. V. Ortiz, J. B. Foresman, C. Y. Peng, P. Y. Ayala, W. Chen, M. **W.** Wong, J. L. Andres, E. S. Replogle, R. Gomperts, R. L. Martin, D. J. Fox, J. S. Binkley, D. J. Defrees, J. Baker, J. J. P. Stewart, M. Head-Gordon, C. Gonzalez, and J. A. Pople, *GAUSSIAN 94* **(Gaussian,** Pittsburgh, PA, **1995).**
3. R. Steckler, W.-P. Hu, Y.-P. Liu, G. **C.** Lynch, B. C. Garrett, A. D. Isaacson, D.-h. Lu, V. S. Melissas, T. N. Truong, S. N. Rai, G. C. Hancock, J. G. Lauderdale, T. Joseph and D. G. Truhlar, POLYRATE - version **6.5** (University of Minnesota, Minneapolis, **1995).**
4. A. McIlroy and L. K. Johnson, ***Combust. Sci. Tech.*****, 116/117, 31 (1996).**